Fuel cell condition monitoring system based on interconnected DC-DC converter and voltage monitor

Andrej Debenjak[1,2], Janko Petrovčič[1], Pavle Boškoski[1], Bojan Musizza[1], and Đani Juričić[1]

[1]Jožef Stefan Institute, Department of Systems and Control, Jamova cesta 39, SI-1000 Ljubljana, Slovenia
[2]Jožef Stefan International Postgraduate School, Jamova cesta 39, SI-1000 Ljubljana, Slovenia

This paper presents a comprehensive solution for condition monitoring of PEM fuel cell systems. It comprises a modular DC-DC converter, a 90-channel fuel cell voltage monitor, and embedded diagnostics algorithms. Besides its basic functionality, the DC-DC converter is designed to perform diagnostic probing of fuel cells by injecting current excitation waveforms. The designed voltage monitor enables precise voltage measurement of all individual cells in the stack. Interconnected DC-DC converter and voltage monitor provide a platform for an embedded condition monitoring system. It employs a novel algorithm for fast electrochemical impedance estimation and automatic tuning of the thresholds used in the fault detection algorithm. The final output is a unit-free condition indicator that describes the overall health of the fuel cell stack. As such, the designed condition monitoring system allows seamless integration and optimal exploitation of fuel cell power systems. The complete solution has been evaluated on an 8.5 kW PEM fuel cell power system.

***Index Terms*—DC-DC Converter, Voltage Monitor, Condition Monitoring, PEM Fuel Cell, PRBS, Continuous Wavelet Transform**

I. INTRODUCTION

BY its very nature, the proton exchange membrane (PEM) fuel cell technology offers efficient energy conversion along with low environmental footprint [1]. The energy conversion is done through electrochemical reaction of combining hydrogen and oxygen at peak efficiency of 55% [2, 3]. High conversion efficiency combined with no green-house emissions are promoting PEM fuel cells as an energy source of the future.

A set of supporting subsystems is a prerequisite for the optimal exploitation of PEM fuel cells. This set comprises, but is not limited to, balance of plant (BoP) components, direct-current-to-direct-current (DC-DC) converter, precise voltage monitor, and supervisory control unit [4–6]. On top of these hardware subsystems, an effective online condition monitoring (CM) system enables real-time assessment of fuel cell health. A typical structure of such a PEM fuel cell-based system is presented in Fig. **??**.

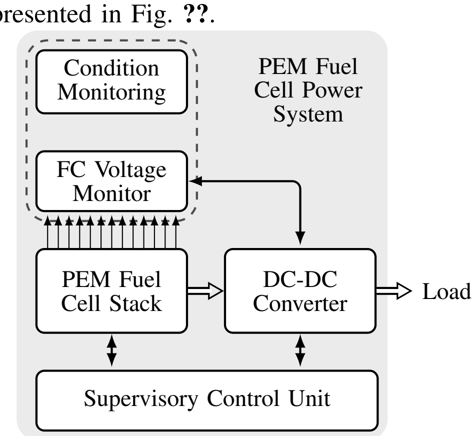

Contemporary commercial fuel cell systems are equipped with DC-DC converters and voltage monitors that fulfill only basic requirements for output power conditioning (e.g., [7–13]) and monitoring (e.g., [14, 15]), respectively. Such systems fail in providing accurate information about system condition. The diagnostic aspect is of a significant practical merit, since the durability and reliability of PEM fuel cells are vitally influenced by several kinds of faults [16, 17]. Therefore, timely and precise information about the health condition of the fuel cell system allows optimal exploitation with respect to its momentary capabilities in various applications (e.g., [18–21]).

All things considered, the aim of the present study is to bridge the gap between the laboratory-grade measurement equipment and contemporary commercial diagnostic systems. The designed electronics employ innovative design solutions by employing industry-standard components. Consequently, the constructed system is both (i) commercially viable and (ii) precise enough to perform sophisticated diagnostic measurements. The combination of the designed DC-DC converter with the 90-channel fuel cell voltage monitor (FCVM) represents a capable platform for accurate online CM. Hence, this paper addresses the following subsystems:

- a DC-DC converter with the capability of generating probing signals for diagnostic purposes
- a 90-channel FCVM capable of precise voltage measurement of each cell of a fuel cell stack and extraction of small voltage variations
- an algorithm for fast impedance estimation by employing pseudo-random binary sequence (PRBS) signal
- a systematic approach for tuning of the threshold of the CM system and calculation of an overall unit-free condition indicator (CI)

Deterioration in operation conditions (i.e., presence of faults) of PEM fuel cells affects their electrochemical impedance characteristic. Consequently, faults can be detected with a multitude of approaches based on electrochemical

Corresponding author: A. Debenjak (email: andrej.debenjak@ijs.si).

impedance spectroscopy (EIS) [22–27]. Despite the sufficiently high diagnostic resolution of this technique, two obstacles hinder the usage of EIS for online CM system:

1) typical EIS estimation using single-sine excitation signals is time consuming (typically a few minutes) and is therefore unsuitable for fast online condition monitoring purposes
2) proper selection of diagnostic threshold requires a rich set of historical records at various conditions of fuel cell system

To address the first issue, an algorithm for fast estimation of the fuel cell impedance was developed that employs small-amplitude PRBS excitation signal with a duration of less than 60 seconds. The DC-DC converter superimposes the PRBS excitation signal onto the stack electrical current. Using the FCVM for data acquisition and signal processing, the impedance is estimated using continuous wavelet transform (CWT) with the complex Morlet mother wavelet [28].

With regard to the second issue, the thresholds of the CM system can be easily determined by employing the probability of false alarm (PFA) through the analysis of the statistical properties of the electrical impedance at different frequencies [29]. As a result, a unit-free CI is obtained whose value is directly related to the overall condition of the fuel cell system.

For the purpose of the complete system presentation, first the hardware components are presented: DC-DC converter in Section II and FCVM in Section III. Afterward, a brief overview of the method for fast impedance estimation using CWT as well as implementation of the CM algorithms are given in Section IV. Finally, the evaluation results are presented in Section V.

II. DC-DC CONVERTER

The presented DC-DC converter is a conversion module that converts the output voltage of a fuel cell power module to the voltage of an energy storage device (e.g., rechargeable lithium battery or storage capacitor). The input device (i.e., fuel cell stack) and the output device (i.e., secondary battery) are current source and current drain, respectively. Therefore, the DC-DC converter should be treated and designed as a current-transforming device. Yet this is uncommon for nearly all commercially available converters, which mostly operate as voltage-transforming devices.

[1]The DC-DC converter targets medium power, stationary auxiliary and uninterruptible power supply applications, where the power bus voltage is lower that the output voltage of the fuel cell stack. This dictates the use of the step-down DC-DC converter topology. However, the use of the step-up topology would have some benefits in comparison to the step-down one. For the solutions presented in this paper, the most notable would be a direct input current modulation and low input (i.e., fuel cell stack) current ripple. As a consequence of a lower current ripple, a smaller input capacitor bank would be required. The step-up topology is of a great interest in automotive, aviation and other fields of applications. However, the overall system design in the presented case requires use of less favorable topology.

The DC-DC converter module presented in this paper is designed as a current-transforming device. Consequently, the stack current is under the primary control, while the stack voltage is monitored in order to ensure safety and operation in an appropriate range. The same applies to the output side, where the current is under primary control, and the output voltage is supervised in order to stay in the predefined range.

To achieve high conversion efficiency, a topology with the lowest number of power components is preferred. The conversion topology employed is the step-down converter. For such a converter, the main energy flow goes only through a single pole–double throw electronic switch and the power inductor. As a result, only a small amount of energy is cycled in the power inductor during each conversion cycle.

This topology suffers from three drawbacks: (i) the input voltage must always be higher than the output voltage, (ii) the input and output ports are not galvanically separated, and (iii) the input current ripple is high. The first issue is not critical for medium size power systems with stacks comprising 50 to 100 cells. The second one can be overcome, as fuel cell stacks can be made electrically floating or grounded at one side. The third one is of real concern, and it has to be properly handled, since ripple current at the input side negatively affects the fuel cell stack. The ripple influence is effectively mitigated by use of electrolytic capacitor bank at the input side of the DC-DC converter.

[2]It should be noted that the electrolytic capacitors may be easily replaced with the power-film ones [30, 31]. This would enhance the reliability of the system and reduce the weight, which is particularly beneficial for transportation applications. The usage of power-film capacitors would be even more justified in the case of the step-up DC-DC conversion topology because of higher voltages [30].

Given the current mode of operation, several DC-DC converter modules can be paralleled to obtain higher output currents. The external master controller can be programmed to dynamically share the load between several parallel converters in order to fulfill the current load requirements and to optimize the efficiency of conversion. [3]At low current loads, the master controller can switch off some of the modules and drive the others to a higher conversion power. In this way, the switching losses of the less loaded modules are eliminated and the overall conversion efficiency is increased.

In the present configuration, the solution is limited to a maximum of eight parallel DC-DC converter modules, each handling up to 80 A of output current. When eight units are paralleled, the overall current reaches up to 640 A, attaining the capacity of power conversion of near 16 kW in 24 V systems. An example of implemented 5 kW conversion block is shown in Fig. 1. The assembly consists of three parallel DC-DC converter modules, two capable of delivering 80 A and one 40 A of current.

[4]By paralleling several DC-DC converter modules, a lower

[1]Reviewer #3, question 3.5.

[2]Reviewer #3, question 3.6.

[3]Reviewer #5, questions 5.2.

[4]Reviewer #5, questions 5.1.

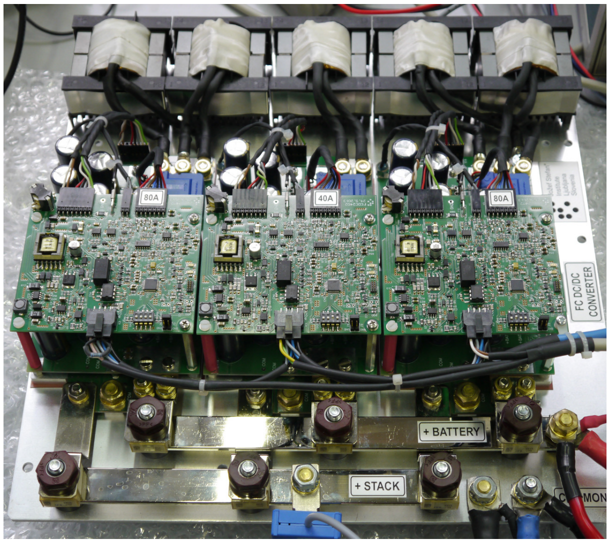

Fig. 1: Assembly of three DC-DC converter modules paralleled together providing 5 kW of power conversion capability.

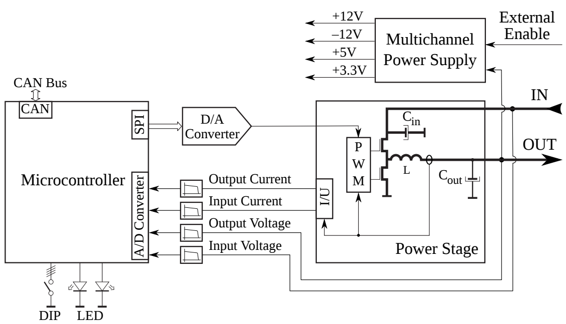

Fig. 2: Block diagram of the DC-DC module.

input current ripple is achieved by the asynchronously operated modules. The current mode step-down converter with constant OFF-time inherently operates with variable frequency. As confirmed by the performed test, three paralleled modules have never fallen into synchronism, even if they were driven by the same current set-point. This allows further optimization (i.e., reduction) of the size of the input capacitor bank.

The block diagram in Fig. 2 depicts the conceptual arrangement of the DC-DC module. Roughly, the module can be divided into three functional blocks, namely,

- multichannel power supply,
- microcontroller circuitry, and
- step-down power output stage.

A. Microcontroller circuitry

The microcontroller circuitry is powered by a multichannel power supply. The supply voltages are generated by a flyback converter topology. The multichannel power supply must be enabled by an external digital signal. With this signal, the external master controller can switch ON or OFF the complete DC-DC converter module. This enables isolation of the defective module as well as increase the efficiency of operation at low loads.

The DC-DC module is managed over a controller area network (CAN) bus communication line. The primary task of the microcontroller is to receive CAN messages with set-point values for the DC-DC converter and to adjust the peak current of the output stage accordingly. [5]The set-points that can be sent to the microcontroler of a DC-DC converter module via the CAN bus are: (i) the peak value of the output current, (ii) the maximum output voltage, (iii) the amplitude of the excitation signal for the impedance measurements, and (iv) the frequency of the excitation signal. The only way the embedded microcontroller can affect the power stage is by means of a control signal through an external 12-bit D/A converter. The microcontroller supervises the operation of the DC-DC conversion across four analogue inputs (see Fig. 2).

B. Power output stage

The step-down power output stage is designed as a self-sufficient block. It needs no microcontroller intervention to oscillate and to control the output current. Hence, the safety of the power control is not affected by possible software errors or strong external transients, which would cause the microcontroller to operate temporally in an undefined state.

The energy flow of the power output stage of the DC-DC converter is controlled by pulse-width modulation (PWM). The design of the output stage is presented in Fig. 3. PWM cycles power metal-oxide-semiconductor field-effect transistors (MOSFETs) in a synchronous mode. This mode reduces power dissipation during the OFF cycle of the converter. Power inductor L filters the modulating current variations and, together with the output capacitor C_{out}, provides necessary low-pass filtering. Input current variations are filtered out with input capacitor bank C_{in}, which eliminates fuel cell stack current ripple. Stack current is delivered through the Schottky diode D_1 intended to prevent back current flow that would otherwise cause an irreparable damage to the fuel cell stack.

The standard current mode converter with constant frequency is most often employed, although it suffers from the inherent low-frequency instability [32–35]. As the stack voltage is frequently close to the required output voltage, the DC-DC conversion is subjected to operation at high PWM duty cycles. The constant-OFF mode of the current control is a particularly convenient method for this purpose. Therefore, at the design of the DC-DC converter, a *current mode step-down converter with a constant OFF-time and synchronous switching mode* was used. The constant-OFF type encounters no inherent instability problems and enables cycle-by-cycle peak current control of the output stage.

Fig. 3 shows that the output pair of N-type MOSFETs is driven by a high-side/low-side MOSFET driver. When the upper MOSFET bank is switched ON, electrical current starts to flow from the fuel cell stack and the input capacitor bank into the output capacitor bank and the load. The current in the inductor increases until the current sensor detects a set-point value, as shown in Fig. 4. When output current exceeds the set-point value, the Comp$_1$ triggers the monostable flip-flop. This causes the top MOSFET bank to switch OFF and the

[5]Reviewer #5, questions 5.3.

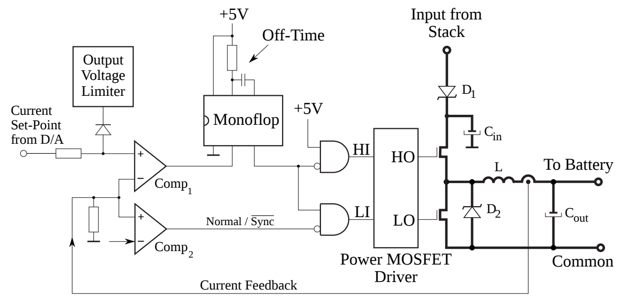

Fig. 3: Power output stage of the current-mode DC-DC converter.

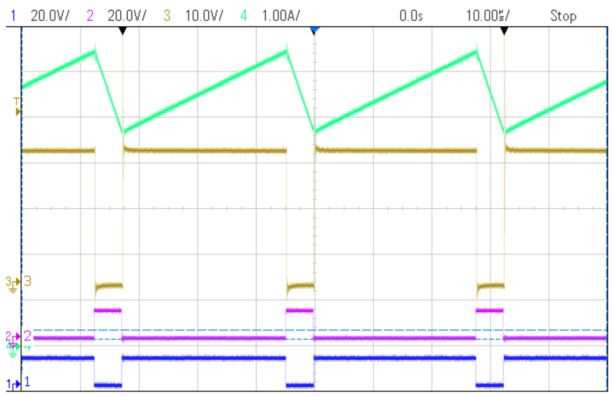

(a) U_{in} = 32 V, I_{out} = 5.5 A

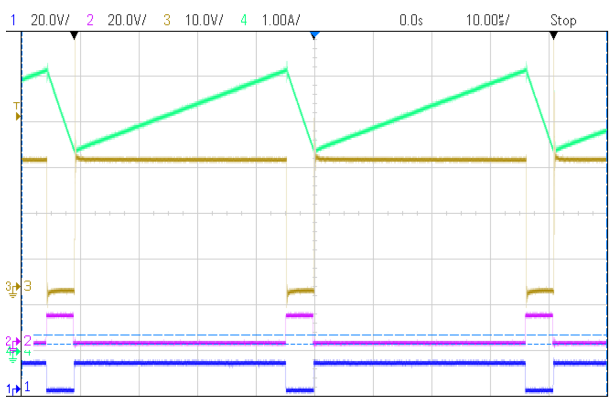

(b) U_{in} = 28 V, I_{out} = 5.5 A

Fig. 4: Key waveforms of the DC-DC converter operating at two different input voltages U_{in} and the same output current I_{out} (CH1[blue]: LI signal, CH2[magenta]: HI signal, CH3[brown]: voltage of the power inductor's entry point, CH4[cyan]: power inductor current).

bottom MOSFET bank to switch ON (the driving signals for the MOSFET banks are shown in Fig. 4). The inductor current recirculates through the lower transistor bank and decreases linearly for a defined amount of time (constant-OFF). When the predefined time elapses, the top MOSFETs switch ON again and allow the passage of stack current to the output.

The OFF-time is determined by the RC constant of the monoflop constant. The ON-time is variable and depends on the input voltage. If the input voltage from the stack is high, the ON-time becomes short, and vice versa. When the input voltage approaches the output voltage, the oscillation ceases away, and the current goes straight through. [6]With the present design, the OFF-time is set to 4 μs. When the fuel cell stack output voltage is near twice the required DC-DC converter output voltage, the output stage oscillates at 125 kHz. The switching frequency increases with the input-output voltage ratio. When the input voltage is only a few volts above the output voltage, the switching frequency drops to a few kilohertz. At the ultimate situation, the switching stops completely. In this way, a very wide range of input voltages are covered. Given the back flow protection diode D_1, the input voltage must be at least one diode drop higher than the output voltage. To illustrate the constant-OFF mode, the waveforms shown in Fig. 4 were acquired under the same output current I_{out} but at two different input voltages U_{in}. The OFF-time is identical in both cases, whereas the ON-time is longer in the case of lower input voltage U_{in} (i.e., Fig. 4b) in order to fulfill the requirements of the output current.

When a battery is connected to the output of the converter, the implementation of the synchronous mode is not a straightforward task. The back-flow current might flow from the battery back through the power inductor and the lower bank of MOSFETs (e.g., at zero current set-point). In such a case, the inductor current would rise to values, at which the circuitry would be damaged instantly. To avoid this, the circuitry actually switches between the normal mode (when the diode D_2 is used to recirculate the inductor current) and the synchronous mode (when low side MOSFETs are used instead). The switch-over is performed by the comparator Comp_2. At low output current, the output stage operates in normal mode, and lower MOSFETs are never switched ON. At higher output currents, the synchronous mode takes over and keeps the switching looses low.

The DC-DC converter strictly operates in current-transforming mode. However, when the output voltage reaches the gassing level of the battery, the output current is reduced. In this situation, the output voltage limiter (see Fig. 3) reduces the current set-point. It operates as a secondary voltage control loop and fixes the battery voltage at the set-value by forcing lower output current as demanded.

III. Fuel cell voltage monitor

A significant voltage drop is an indication that either the operating conditions or the health of the fuel cell are seriously impaired. Therefore, even low-cost fuel cell-based power systems require some kind of cell voltage monitoring. A significant discrepancy exists between the laboratory-grade and commercially available diagnostic and measurement equipment. The trade-off is between the capability of handling fast and precise measurements on one hand and the price on the other [36, 37]. Most of the commercially installed FCVM systems are capable of measuring only the joint voltage of two or more adjacent fuel cells with rather low sample rate and resolution. Notwithstanding the cost-effectiveness, such equipment suffices only for detecting severe deteriorations in the fuel cell condition. As a result, it is incapable of performing

[6]Reviewer #5, questions 5.4.

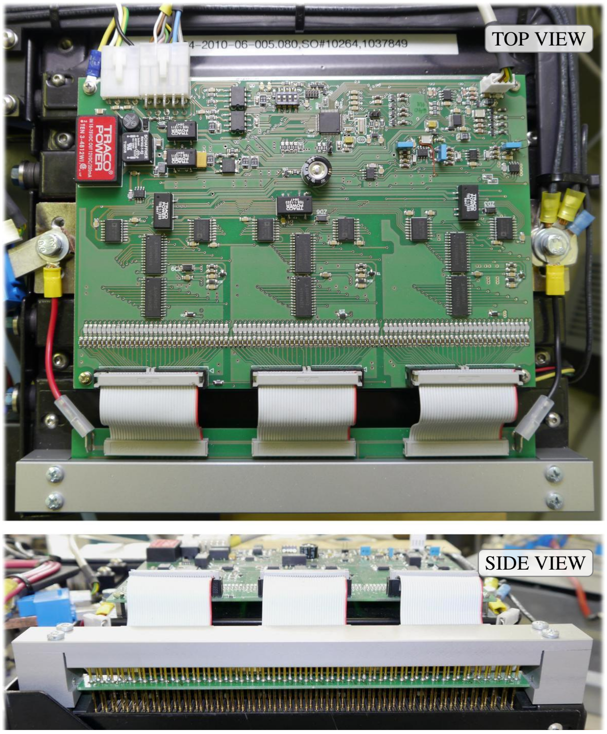

Fig. 5: FCVM connected to an 8.5 kW PEM fuel cell system Hydrogenics HyPM-HD 8-200 (top view: FCVM's PCB; side view: realization of contacts to all of the fuel cells).

total stack monitoring or providing more sophisticated diagnostic information.

The proposed solution bridges the gap between the laboratory-grade measurement equipment and contemporary commercial diagnostic systems. The proposed FCVM is a low-cost data acquisition device capable of performing precise voltage measurement of individual cells inside a fuel cell stack that consists of up to 90 cells. Additionally, it provides a platform for conducting EIS measurements on every cell of the stack. Fig. 5 shows a typical implementation of the FCVM connected to a PEM fuel cell stack of a commercially available power unit via spring contact pins.

A. Resolving high common-mode voltage potential issue

One of the biggest issues when measuring the voltage of an individual cell within a larger stack is a high common-mode potential, which builds up from the potentially low cell to the highest cell in the stack. The signal acquisition system must be capable of measuring only a few hundred millivolts superimposed on several tens of volts. Such high common-mode potential poses two limiting factors: the ability of a multiplexer to select the individual cell within this very wide common-mode voltage range and the ability of instrumentation amplifiers or floating A/D converters to extract the relatively small cell voltage in the presence of high voltage offset [38].

The issue of high common-mode voltage range of multiplexers remains unsolved by readily available low-cost measurement devices. The proposed solution employs standard CMOS analogue multiplexers. By proper biasing and using an isolated DC-DC power supply, making an analogue multiplexer floating is possible. Fig. 6 shows that an isolated DC-DC converter provides voltage supply to the multiplexer. Two Zener diodes regulates the bias for the multiplexer for maximum input range, while an NPN transistor supplies current to a digital signal isolator, which selects the particular input. The selected voltage is then transferred to the difference amplifier for further signal preparation and A/D conversion. One such circuitry is capable of handling signals from up to 30 fuel cells.

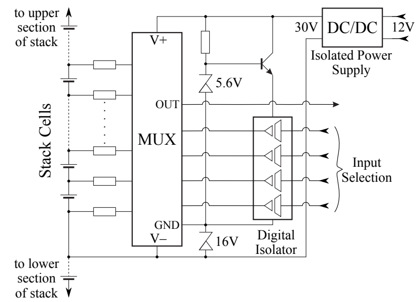

Fig. 6: Floating power supply scheme, which allows industry-standard multiplexer to operate in floating mode.

to decrease the number of multiplexers, two multiplexers are interlaced as shown in Fig. 7. In this way, only one input is effectively used per cell. Thus, selecting 30 cells is possible by using a pair of standard 16-to-1 multiplexers. One spare channel is used for automatic auto-zero measurement, which eliminates the offset voltage of the difference amplifier.

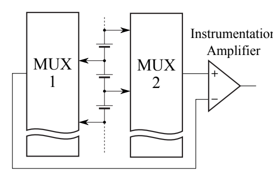

Fig. 7: Connection of two industry-standard multiplexers to measure up to 30 fuel cell leads in order to reduce component count.

An ARM Cortex-based microcontroller performs synchronization among different AD channels required for proper data acquisition. Additionally, the microcontroller controls the communication interfaces and provides the necessary computational resources for execution of the diagnostic algorithms.

B. FCVM measurement modes

The FCVM can perform two types of measurements:

- voltage monitoring of all the cells of the stack
- impedance measurement of individual cells

In the first mode, the FCVM measures the voltage of each individual cell inside a stack with resolution of 62.5 μV. The stack voltage and current are also measured with a resolution of 24 mV and 10 mA, respectively. The stack voltage and current are measured through simple voltage divider and Hall-effect current transducer, respectively. In the monitoring mode, the refresh rate is 400 ms.

The second measurement mode provides a powerful tool for performing measurements intended for EIS-based diagnostics. The relevant AC diagnostic signals are superimposed to the operational DC signals of the fuel cell and have small amplitudes with respect to the DC component. Measuring such low amplitude AC signals at low noise is of utmost importance.

To achieve the required high resolution at low noise, the voltage of an individual cell undergoes two preprocessing steps. In the first step, the DC component is subtracted by employing the analogue subtraction circuit. In the second step, the remaining AC component of the signal is amplified by a factor of 10 in order to attain low noise and higher resolution of A/D conversion, as shown in Fig. 8. Consequently, the FCVM measures the AC voltage of sequentially selected cells inside a stack with a high resolution of 80 μV at a sampling rate of 5 kHz. A special care was taken to keep frequency response of voltage and current measuring paths as equal as possible as the impedance is actually proportional to their ratio in amplitude/phase space.

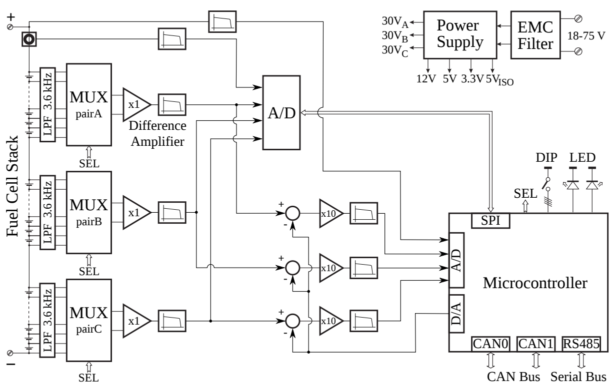

Fig. 8: Block diagram of the FCVM.

Normally, extraction of AC signals in the presence of DC signal is performed by using a high-pass analogue filter. However, switching among cells would cause long settling time of the filter, which would significantly prolong the data acquisition time. Since the DC voltage of the cell, obtained by the first measuring mode, is already known to the microcontroller, the value is sent to the subtraction circuitry via the D/A converter, as shown in Fig. 8. The result is the AC component of the signal with a small DC residue caused by circuit imperfections and slow cell voltage variations. This composite signal is then amplified to gain higher resolution and to keep high signal-to-noise ratio. As DC residue is also amplified, it is removed later by digital signal processing within the microcontroller.

C. DC-DC converter and FCVM as a condition monitoring system

To perform online EIS-based CM of PEM fuel cells, the DC-DC converter module and the FCVM were interconnected into a CM system. The interconnection enables to conduct measurements that are required for a fast online estimation of the impedance of PEM fuel cells. The FCVM manages the estimation procedure, performs the voltage and current measurements, and conducts the signal processing tasks. The DC-DC converter perform the DC-DC conversion, and when prompted by the FCVM, it executes the current excitation of fuel cells. The scheme of the interconnected condition monitoring system is shown in Fig. 9.

[7a] To perform the current excitation of the cells, the DC-DC converter module is equipped with a firmware-based excitation pattern generator, as shown in Fig. 9. Using the selected pattern, the microcontroller modulates the output current of the DC-DC converter. As this variation of the output current is filtered out by the output capacitor bank, the modulation is not affecting the load significantly. On the input side of the DC-DC converter, the current modulation affects the current through the fuel cell stack. The stack becomes excited enough to respond with minute variations of the cells' voltages. By measuring these variations with the FCVM, the information on the impedance of the cells is obtained.

The excitation of the fuel cell stack is affected by the presence of the input capacitor bank of the DC-DC converter and its dynamics. The capacitor bank must be present to reduce stack current ripple. This capacitance is paralleled to the stack and its influence is most prominent at high frequencies, while the information on the cells' condition is present at low frequencies.

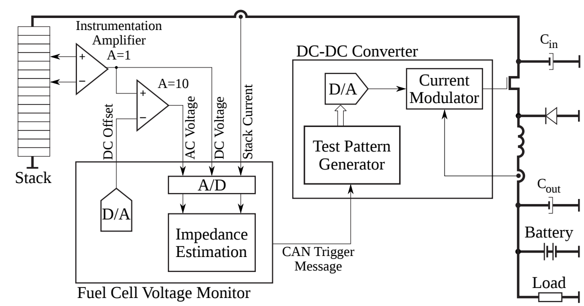

Fig. 9: Connection scheme between the FCVM and the DC-DC converter for online condition monitoring.

IV. Condition Monitoring

The embedded CM approach builds on top of a method for fast impedance estimation [28]. This method employs PRBS excitation signal and CWT signal processing tool. It enables substantially faster estimation of PEM fuel cell impedance characteristic compared to other conventional methods, which utilize single-sine signals. Due to the specific statistical properties of the PRBS waveform, the CM thresholds are determined based on the probability distribution of impedance at particular frequencies and desired value of PFA [29]. Finally, a unit-free CI indicator is formulated, which provides an overall assessment of the PEM fuel cell condition.

A. Fast impedance estimation using CWT and PRBS

1) CWT based on the complex Morlet wavelet

Following the procedure described by Debenjak et al. [28], the impedance characteristic can be efficiently estimated by

[7]Reviewer #3, question 3.2 (the comments are split between sections III-C and V-A.

using complex wavelet coefficients of the CWT of the fuel cell's current $i(t)$ and voltage $u(t)$ using the complex Morlet mother wavelet. The CWT of a square integrable function $f(t) \in \mathbf{L}^2(\mathbb{R})$ is defined as follows [39]:

$$Wf(u,s) = \langle f(t), \psi_{u,s}(t) \rangle = \int_{-\infty}^{\infty} f(t)\psi^*_{u,s}(t)\,dt, \qquad (1)$$

where $\psi_{u,s}(t)$ is a scaled and translated version of the mother wavelet $\psi(t)$:

$$\psi_{u,s}(t) = \frac{1}{\sqrt{s}}\psi\left(\frac{t-u}{s}\right), \qquad (2)$$

which in the present study is the complex Morlet wavelet with parameter ω_0 [40]:

$$\psi(t) = \pi^{-1/4}\left(e^{-j\omega_0 t} - e^{-\omega_0^2/2}\right)e^{-t^2/2}. \qquad (3)$$

The wavelet coefficients (1) fully characterize the analyzed signal $f(t)$ on the time-scale plane. The translation between scale s and frequency f is straightforward by using the following [39]:

$$\frac{1}{f} = \frac{4\pi s}{\omega_0 + \sqrt{2+\omega_0^2}}. \qquad (4)$$

Therefore, in the remainder of the paper, all subsequent relations will rely on actual frequency f.

2) PRBS as excitation signal

PRBS can be regarded as sufficiently close to stationary random noise with power spectral density similar to that of white noise. Furthermore, the probability distribution of the amplitude of its frequency components can be regarded as Gaussian [41]. Analyzing such a signal with CWT preserves its statistical properties within the wavelet coefficients. As the DC-DC converter superimposes the PRBS signal on the current $i(t)$ drawn by the load, the voltage $u(t)$ will response accordingly. Analyzing both signals with CWT results into wavelet coefficients:

$$\begin{aligned} Wi(t,f) &= \Re\{Wi(t,f)\} + j\Im\{Wi(t,f)\}, \\ Wu(t,f) &= \Re\{Wu(t,f)\} + j\Im\{Wu(t,f)\}. \end{aligned} \qquad (5)$$

Impedance at a particular frequency can be regarded as zero-mean Gaussian circular complex random variable [42]. Therefore, the complex wavelet coefficients have the following properties:

$$\begin{aligned} \Re\{Wi(t,f)\}, \Im\{Wi(t,f)\} &\sim \mathcal{N}\left(0, \frac{\sigma_i^2}{2}\right), \\ \Re\{Wu(t,f)\}, \Im\{Wu(t,f)\} &\sim \mathcal{N}\left(0, \frac{\sigma_u^2}{2}\right), \end{aligned} \qquad (6)$$

where the corresponding variances σ_u^2 and σ_i^2 are parameters that should be estimated. Using the complex wavelet coefficients (6), the impedance at particular frequency $f = f_0$ can be calculated as a ratio of the complex wavelet coefficients:

$$z(t) = \left.\frac{Wu(t,f)}{Wi(t,f)}\right|_{f=f_0} = z_r(t) + jz_i(t). \qquad (7)$$

B. Probability density function of the complex impedance $z(t)$

Current $i(t)$ and voltage $u(t)$ in (7) are correlated, which can be expressed with the covariance matrix [43–45]:

$$\Sigma = \frac{1}{2}\begin{bmatrix} \sigma_u^2 & \rho\sigma_u\sigma_i \\ \rho^*\sigma_u\sigma_i & \sigma_i^2 \end{bmatrix}, \qquad (8)$$

where $\rho = \rho_r + j\rho_i$ is complex correlation coefficient, such that $|\rho| \leq 1$. As a result, the probability density function (PDF) of the ratio (7) reads as follows [46]:

$$p_z(z) = \frac{1-|\rho|^2}{\pi\sigma_u^2\sigma_i^2}\left(\frac{|z|^2}{\sigma_u^2} + \frac{1}{\sigma_i^2} - 2\frac{\rho_r z_r - \rho_i z_i}{\sigma_u\sigma_i}\right)^{-2}. \qquad (9)$$

The distribution of real z_r and imaginary z_i components of the impedance (7) can be derived from the distribution (9). The PDF of the imaginary component z_i reads as follows [46]:

$$p_{z_i}(z_i|\rho_r,\rho_i) = \frac{\left(1-|\rho|^2\right)\sigma_x^2\sigma_y}{2\left(\left(1-\rho_r^2\right)\sigma_x^2 + 2z_i\rho_i\sigma_x\sigma_y + z_i^2\sigma_y^2\right)^{3/2}}. \qquad (10)$$

For the real component z_r, the PDF has the same shape and reads as follows:

$$p_{z_r}(z_r|\rho_r,\rho_i) = p_{z_i}(z_r|-\rho_i,-\rho_r). \qquad (11)$$

Besides the probability distribution of the real z_r and imaginary z_i components of the impedance, in many cases, the module of the complex impedance can be used as a feature in condition monitoring. For the circular Gaussian complex random variables (6), the corresponding modules $|Wu(t,f_0)|$ and $|Wi(t,f_0)|$ are distributed according to Rayleigh distribution:

$$\begin{aligned} |Wu(t,f_0)| &\sim \text{Rayleigh}(\sigma_u), \\ |Wi(t,f_0)| &\sim \text{Rayleigh}(\sigma_i). \end{aligned} \qquad (12)$$

As the current $i(t)$ and voltage $u(t)$ are correlated, the PDF of the module of the ratio (7) reads as follows [47]:

$$p_{|Z|}(|z|) = \frac{2\sigma_i^2\sigma_u^2(1-\rho^2)|z|(\sigma_i^2|z|+\sigma_u^2)}{\left[(\sigma_i^2|z|^2+\sigma_u^2)^2 - 4\rho^2\sigma_u^2\sigma_i^2|z|^2\right]^{3/2}}, |z| \geq 0, \qquad (13)$$

where $|\rho| \leq 1$ is the correlation coefficient, as defined in (8). The probability distribution function (13) is positively skewed and defined on the nonnegative semi-axis. A typical realization of the probability distribution function (13) is shown in Fig. 10.

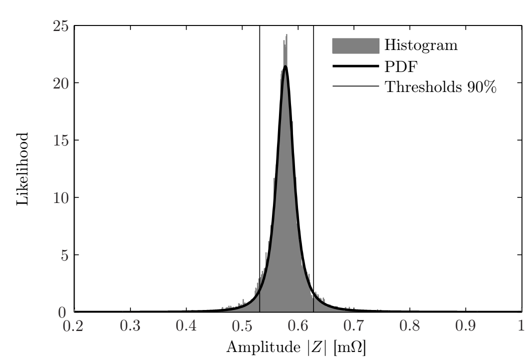

Fig. 10: Probability distribution function of $|Z|$ at 157 Hz.

C. Fuel cell condition indicator based on PFA

Determining the optimal threshold values at which the deterioration can be regarded as significant is of great importance for a condition monitoring system. Too-high thresholds decrease the sensitivity of the diagnostic system to faults and hence increase the probability of missed alarms. At the same time, the probability of false alarms is decreased. Too-low thresholds increase the chances for false alarms, which can easily ruin the credibility of the monitoring system. The most commonly used criterion for determining the thresholds is not by explicitly defining their values, but rather by defining the permitted PFA [48].

A condition monitoring system based on low PFA will raise alarms only when the condition of the fuel cell is suboptimal. Having derived the PDF (13), upper and lower thresholds can be handily found as critical values of a two-sided test using its cumulative distribution function (CDF) $P_{|Z|}(z)$:

$$\begin{aligned} T_{\downarrow} &= P_{|Z|}^{-1}\left(\frac{p_{FA}}{2}\right) = \inf\left\{P_{|Z|}(z) \geq \frac{p_{FA}}{2}\right\}, \\ T_{\uparrow} &= P_{|Z|}^{-1}\left(1-\frac{p_{FA}}{2}\right) = \inf\left\{P_{|Z|}(z) \geq 1-\frac{p_{FA}}{2}\right\}. \end{aligned} \tag{14}$$

Note that expression $\frac{p_{FA}}{2}$ is used to split the PFA between both ends of the PDF, since the presence of different faults can increase or decrease the value of $|z|$. The CDF $P_{|z|}(z)$ that corresponds to (13) reads as follows [47]:

$$P_{|z|}(z) = \frac{1}{2} - \frac{\sigma_u^2 - z^2\sigma_i^2}{2\sqrt{4z^2\left(1-\rho^2\right)\sigma_i^2\sigma_u^2 + \left(\sigma_u^2 - z^2\sigma_i^2\right)^2}}. \tag{15}$$

[8]The steps of the proposed method for threshold selection are listed in Algorithm 1. The threshold values have to be separately calculated for each individual fuel cell. The algorithm has to be performed for each fuel cell only once (e.g., when commissioning a new system), under fault-free conditions. The only design parameter is the desired PFA value.

Algorithm 1 Determining threshold values

1: **Apply** PRBS excitation signal
2: **Measure** voltage $u(t)$ and current $i(t)$ signals under fault-free condition
3: **Estimate** impedance $z(t)$ using (7)
4: **Estimate** covariance Σ using (8)
5: **Compute** CM thresholds (14) using CDF (15) and the desired PFA value

Condition indicator: Selected threshold values (14) can be additionally employed for mapping the complex impedance values into an so-called CI, which is an abstract feature that can be directly related to the condition of the system [48]. For a healthy system, CI should acquire low values (i.e., $CI = 0$). As the condition deteriorates, the value of CI should increase in accordance with the severity of the fault(s) present in the system. Using PFA value, the values of CI are typically scaled in such a way that values close to one should indicate imminent failure. Thus, CI offers two advantages:

1) it gives a unified and unit-free view of the overall system condition
2) its trend over time can be used for prognostics (i.e., estimation of the remaining useful life[9])

In the context of fuel cells, the presence of fault can either increase or decrease certain impedance components. Therefore, for a fault-free operation, the value of the CI will be in the middle of the region bounded by thresholds at a certain PFA, as shown in Fig. 10.

The mapping into the corresponding CI can be achieved by using the CDF (15). As a result, the impedance components of the fault-free region will acquire values in the vicinity of $1/2$. Setting the maximal value for the CI to be the chosen PFA, the final scaling relation reads as follows:

$$CI = 2 \times (1-p_{FA})^{-1}\left|P_{|Z|}(z) - \frac{1}{2}\right|, \tag{16}$$

where $F_{|Z|}(z)$ is the CDF of the corresponding impedance component.

D. Computationally efficient CWT with the Morlet wavelet

By substituting the mother wavelet $\psi(t)$ with

$$\tilde{\psi}_s(t) = \frac{1}{\sqrt{s}}\psi^*\left(-\frac{t}{s}\right), \tag{17}$$

the relation (1) transforms into the following convolution:

$$Wf(u,s) = \frac{1}{\sqrt{s}}\int_{-\infty}^{\infty} f(t)\tilde{\psi}_s(u-t)\,dt. \tag{18}$$

In the Fourier domain, the convolution (18) becomes

$$Wf(u,s) = \frac{1}{2\pi}\int_{-\infty}^{\infty} \hat{f}(\omega)\sqrt{s}\hat{\psi}(s\omega)e^{j\omega u}d\omega, \tag{19}$$

where $\hat{f}(\omega)$ is the Fourier transform of the original signal $f(t)$ and $\hat{\psi}(\omega)$ is the Fourier transform of the Morlet wavelet (3) [40]:

$$\hat{\psi}(\omega) = \pi^{-\frac{1}{4}}\left(e^{-\frac{(\omega-\omega_0)^2}{2}} - e^{-\frac{\omega^2}{2}}e^{-\frac{\omega_0^2}{2}}\right). \tag{20}$$

V. Experimental validation

[10]Among other faults, the water management ones vitally affect PEM fuel cell operation reliability and efficiency [17]. The diagnosis of these faults is of great practical value, providing information for efficient fuel cell system management. For validation of the proposed CM solution, a commercial PEM fuel cell system was employed, which was subjected to water management faults.

A number of studies show that the water management faults affect the electrochemical impedance of a PEM fuel cell, and therefore can be detected by utilizing EIS-based approaches [49–56]. Water content affects the transport of the involved chemical species (i.e., reactant gases and protons) in different ways [22, 27]. In the case of flooding, the formed water droplets block the pathways to the reaction sites and

[8]Reviewer #5, questions 5.8.

[9]The problems of prognostics are not treated by this paper.

[10]Reviewer #1, question 1.1.

thus preventing the oxygen from being involved and consumed as a reactant. Conversely, when the water level is low, the membrane of a PEM fuel cell is subjected to drying. The PEM is made of an ionomer that has to be sufficiently hydrated in order to conduct protons. If the cell is subjected to drying, the water content of the PEM is reduced and consequently the proton conductivity of the membrane is decreased. Additionally, due to a lower water content, the volume of the ionomer is reduced and it results in a decrease of the contact surface area.

A. Experimental procedure

During the experiments, the fuel cell system was kept at constant operating and environmental conditions. The DC current operating point I_{dc} was set to 70 A, [11]whereas the peak-to-peak amplitude of the superimposed PRBS waveform was set to 4 A. On the one hand, such an amplitude was high enough to sufficiently perturb the PEM fuel cells in order to obtain reliable impedance estimations, and on the other, small enough not to cause difficulties due to nonlinearity of the PEM fuel cells.

[12]The frequency f_s of the PRBS excitation signal was set to 600 Hz. The frequency f_s defines the rate at which the PRBS signal can switch its value. In other words, the value of the signal can change every 1.67 ms ($\Delta t = 1/f_s$). According to the theory, the PRBS signal has nonzero power spectrum (and therefore provides the excitation energy) at all frequencies, except at those with values of integer multiples of the frequency f_s [57, pp. 164–172]. However, for practical impedance estimation purposes, the useful bandwidth f_B of the PRBS excitation signal is limited to approximately one third of the frequency f_s ($f_B \simeq f_s/3$) [28]. For the case at hand, the useful frequency band f_B covers frequencies from 0 to approximately 200 Hz. On the other hand, the data acquisition sampling frequency f_{DAQ}, at witch the voltage and current signals were acquired, was set to 5 kHz. [13]During the experiment, the impedance was estimated every 40 seconds. Within that time interval, the PRBS excitation was applied for 10 seconds. At the same time, the required voltage and current signals were acquired.

Fig. 11 shows an example of the current and voltage signals of a PEM fuel cell during the experiment, which were acquired by the FCVM and used for the impedance estimation. [7b]As can be seen from Fig. 11, the actual fuel cell current is not of an ideal PRBS waveform. The shape is affected by the presence of the input capacitor bank of the DC-DC converter and its dynamics, as discussed in Subsection III-C. It should be stressed that the proposed impedance estimation method (i.e., CWT-based signal processing) does neither assume nor require that the current is of pure PRBS waveform. Based on the actual frequency components in the voltage and current signals, the method estimates the impedance and provides the corresponding confidence intervals of the estimation. However, the CI methodology assumes the complex circularity of the signals' frequency components (presented in section IV-A2). The PRBS comply with the requirement and the circularity is retained as long as the signal is subjected to any kind of linear transformation. Consequently, the CI methodology is capable of handling affected PRBS signals as long as the DC-DC converter does not modify them in a nonlinear fashion.

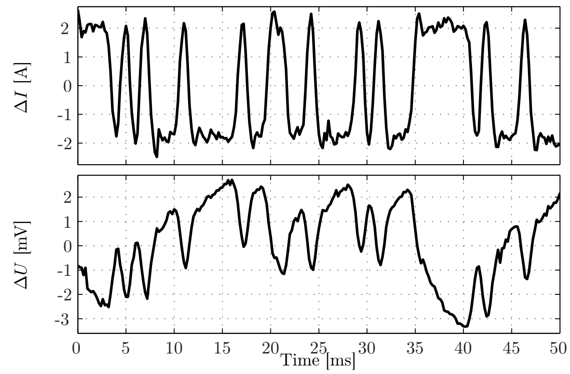

Fig. 11: Example of acquired current and voltage signals.

The experiment went through five stages: fault free, dried, fault free, flooded, and back to fault free. The first fault-free stage lasted 10 minutes during which the relative humidity of the inlet air was kept at 10%. During the second stage, between the 10th and the 17th minute, the air fed to the fuel cell was dried down to relative humidity of 2%. Afterward, the inlet air was humidified back to 10% relative humidity to simulate fault-free stage again. In the fourth stage, between the 30th and the 47th minute, saturated air with relative humidity of 100% was fed into the fuel cell system, inducing flooding of fuel cells. Finally, the air humidity was decreased down to the initial 10%. Such an experiment profile enables analysis of the fuel cell response under different fault scenarios with various fault severities. These stages of the experiment are clearly indicated in Fig. 12.

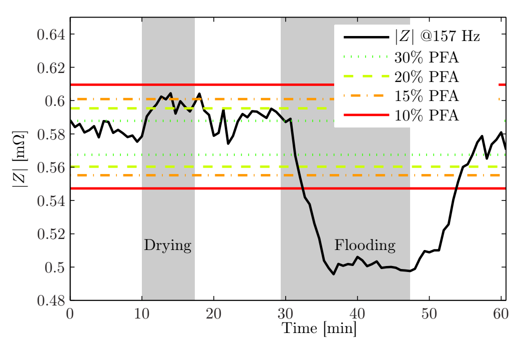

Fig. 12: Trend of $|Z|$ at 157 Hz throughout the experiment.

B. Time evolution of particular impedance components

[14]The parameters ρ, σ_u^2, and σ_i^2 of the PDF (13) were estimated at a frequency of 157 Hz. Note that the exact value

[11]Reviewer #3, question 3.1 (part related to the amplitude of the excitation signal).

[12]Reviewer #5, questions 5.5, 5.6. and 5.7

[13]Reviewer #3, question 3.7.

[14]Reviewer #3, question 3.1 (part related to the frequency at which the impedance was estimated).

of the selected frequency is the consequence of the parameters chosen for the CWT. The proposed CM algorithm performs efficiently also if any other frequency in the range between 10 and 200 Hz is selected. Based on the estimated parameters, the threshold values were calculated at four different $PFA = \{25\%, 20\%, 15\%, 10\%\}$. The resulting CM thresholds and the trend of $|z|$ at the selected frequency are shown in Fig. 12.

The time evolution of $|z|$ corresponds with the five experiment stages, as shown in Fig. 12. The shaded regions mark the occurrence of drying and flooding of the fuel cell. In the drying region, the module of the impedance increased and surpassed the threshold of 70%. Despite the minute changes in the relative humidity of the inflow air, there are clear changes in the value of the impedance, with 30% probability of false alarm. Unlike the minor changes caused by the mild decrease in the humidity, the flooding with 100% saturated air inflow shows significant changes in all three impedance components. The values of $|z|$ indicate that the condition of the fuel cell departed from the fault-free area, with less then 10% PFA. Finally, when the relative humidity of the air inflow was returned to normal, the impedance components returned to the initial values within the fault-free region.

C. Time evolution of the CI

The time evolution of the CI (16) is shown in Fig. 13. The values of the CI were calculated for $PFA = 10\%$. As expected, during the fault-free operation, the CI acquired low values. As the first fault was induced, the values of the CI increased up to 0.5, which indicates deterioration of the fuel cell condition. The acquired value of 0.5 clearly shows departure from fault-free operation while at the same time is in-line with the low severity of the induced drying, relative humidity change of 8%. Unlike the low severity of the drying fault, during the flooding phase of the experiment, the value of CI surpasses the limit value of 1. The overwhelming flooding of the system is directly reflected in the high value of the CI. Finally, at the end of the experiment, when the air condition was back to nominal, the values of CI decreased, indicating an almost fault-free operation.

[15]The results confirm that the CI is sufficiently sensitive to the water management faults. At the same time, the values of the CI are directly related to the severity of the fault. As such, the CI in its present form is applicable for performing fault detection and fault evaluation. In order to perform fault identification and localization, an extension of the proposed CI is required. A possible solution to this problem could be reached by utilization and aggregation of impedance information at multiple frequencies.

VI. Conclusion

This study presents a versatile online condition monitoring system for PEM fuel cells, which builds on integrated DC-DC converter and FCVM. As a result, a fuel cell system is enriched with information about its current health condition, which in essence enables optimal exploitation.

[15]Reviewer #5, questions 5.9.

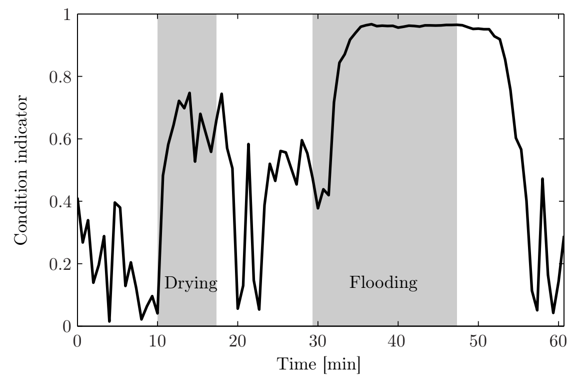

Fig. 13: Trend of CI of $|Z|$ throughout the experiment.

The system encompasses a DC-DC converter with diagnostics capabilities, a 90-channel voltage monitor, and embedded algorithms for signal processing and condition monitoring. The developed DC-DC converter module can be grouped in parallel with what the overall output power is increased. Besides power conditioning, the DC-DC converter enables system probing with arbitrary signals that can be used for diagnostic purposes. Together with the FCVM, it provides the basic hardware platform for online condition monitoring of commercial PEM fuel cell-based power systems. Both devices are built to meet tight requirements regarding size and costs imposed by commercially oriented applications and at the same time to fulfill accuracy requirements set by the diagnostic methodology.

On top of the designed hardware, the online CM system also includes the method for fast estimation of fuel cell impedance. The benefits of the proposed methodologies are twofold. First, it considerably shortens the time required to conduct measurements, which makes it viable for commercial applications. Second, the threshold selection methodology is based on PFA, which enables unambiguous threshold specifications. Based on these thresholds, a unit-free condition indicator is calculated, which describes the overall health of the fuel cell stack. These pieces of information are of significant practical merit for both integrators as well as end users.

The proposed hardware and methodology were validated on a commercially available 8.5 kW PEM fuel cell-based system. The results show that the overall system performs as expected and that it provides the desired information about the operational condition of the system.

Acknowledgment

The authors thank the Slovenian Research Agency (P2–0001) for the financial support.

CVs

Andrej Debenjak received his B.Sc. degree in electrical engineering from the University of Ljubljana, Slovenia, in 2011. Currently, he is employed as a young researcher at the Jožef Stefan Institute, and he is pursuing his Ph.D. degree at the Jožef Stefan International Postgraduate School in Ljubljana, Slovenia.

His research is mainly focused on fault detection and diagnostics of PEM fuel cell systems and prognostics and health management of lithium-based batteries. Areas of his expertise include embedded programming, digital signal processing, statistical analyses, and diagnostics algorithm design. He was involved in the design of an approach for faster estimation of electrochemical impedance with applicability to online diagnostics. He was also responsible for algorithms and firmware design of modular battery management system. Lately, he is working on the design of embedded measurement equipment for fast online impedance estimation of Li-S cells.

Janko Petrovčič joined the Jožef Stefan Institute, Ljubljana, Slovenia, in 1983 and since then works at the Department of Systems and Control. He is currently an R&D advisor.

He received his Ph.D. degree from the Faculty of Electrical and Computer Engineering, University of Ljubljana, Slovenia, in 1992. His main activities are in the fields of process control engineering, process control algorithms, industrial diagnostic, signal acquisition, and electronic design. He works mainly on research and development projects for industry and is responsible for the hardware support of basic research activities of the Department of Systems and Control.

He was leading an electronic design of a control coprocessor module for Mitsubishi Electric Europe. Recently, he led the design of several diagnostic systems for vacuum cleaner and EC motors for Domel d.d., Slovenia. He also participated in the design of new BLDC-driven valve actuators for Danfoss Trata. Currently, he works on FP7 projects, concerning the application of fuel cell-based power systems.

Pavle Boškoski received his B.Sc. in 2002 and Ms.C. in 2007 at the University "Ss. Cyril and Methodius," R. Macedonia. In 2011 he received his Ph.D. with the topic "Condition monitoring of mechanical drives," at the Jožef Stefan International Postgraduate School in Ljubljana, Slovenia. Since 2011, he has been employed at the Jožef Stefan Institute in Ljubljana, Department of Systems and Control. His research work was focused on the development of signal processing methods for prognostics and health management of mechanical drives. Since 2012, his work has been focused on the development of methods for diagnostics of fuel cell-based systems. He authored or coauthored more than 40 journal and conference papers.

Bojan Musizza received his B.Sc. in 2003 and Ph.D. in 2008 with the topic "Methods for analysis of phase interactions and causality analysis between brain and cardio-respiratory oscillations," at the University of Ljubljana. Since 2003, he has been employed at the Jožef Stefan Institute in Ljubljana, Department of Systems and Control. His research work was focused on the development of methods for causality detection between biological oscillators with the application to the problem of depth of anesthesia monitoring. Since 2009, his work has been focused on the development and application of purpose-build electronic modules and software tools for diagnostics and control of fuel cell-based systems, and the development and implementation of signal processing methods for tackling problems in industrial diagnostics. In these fields, he authored or coauthored more than 60 journal and conference papers.

Đani Juričić has earned his Ph.D. in automatic control in 1990 from the University of Ljubljana, Slovenia. Since 1981, he has been affiliated with the Jožef Stefan Institute as head deputy of the Department of Systems and Control. Since 2013, he has been full professor at the University of Nova Gorica, Slovenia. His interests span condition monitoring, with particular focus on fault detection, diagnosis, and prognosis; nonlinear dynamic system identification; statistical signal processing; and optimal control. He has (co)authored more than 200 journal and conference papers with peer review and delivered 10 invited talks. He has been coordinator or person responsible in nearly 40 research projects and projects for the industry. He received several awards, including DAAD Fellowship (2001) and ISA Transactions Best Paper Award for 2009. He is a member of IFAC Technical Committee SAFEPROCESS and a member of the General Assembly and Council of the European Control Association.

References

[1] O. Z. Sharaf and M. F. Orhan, "An overview of fuel cell technology: Fundamentals and applications," *Renewable and Sustainable Energy Reviews*, vol. 32, pp. 810–853, 2014.

[2] F. Barbir, *PEM Fuel Cells: Theory and Practice*. Elsevier, 2005.

[3] V. Jovan, M. Perne, and J. Petrovčič, "An assessment of the energetic flows in a commercial PEM fuel-cell system," *Energy Conversion and Management*, vol. 51, no. 12, pp. 2467–2472, 2010.

[4] X. Yu, M. R. Starke, L. M. Tolbert, and B. Ozpineci, "Fuel cell power conditioning for electric power applications: a summary," *Electric Power Applications, IEEE Transactions of*, vol. 1, no. 5, pp. 643–656, 2007.

[5] L. Palma, M. Harfman Todorovic, and P. Enjeti, "Analysis of common-mode voltage in utility-interactive fuel cell power conditioners," *Industrial Electronics, IEEE Transactions on*, vol. 56, no. 1, pp. 20–27, 2009.

[6] S. N. Motapon, L. A. Dessaint, and K. Al-Haddad, "A comparative study of energy management schemes for a fuel-cell hybrid emergency power system of more-electric aircraft," *Industrial Electronics, IEEE Transactions on*, vol. 61, no. 3, pp. 1320–1334, 2014.

[7] R. J. Wai, C. Y. Lin, R. Y. Duan, and Y. R. Chang, "High-efficiency DC-DC converter with high voltage gain and reduced switch stress," *Industrial Electronics, IEEE Transactions on*, vol. 54, no. 1, pp. 354–364, 2007.

[8] M. Harfman Todorovic, L. Palma, and P. Enjeti, "Design of a wide input range DC-DC converter with a robust power control scheme suitable for fuel cell power conversion," *Industrial Electronics, IEEE Transactions on*, no. 3, pp. 1247–1255, 2008.

[9] G. Wu, X. Ruan, and Z. Ye, "Non-isolated high step-up DC-DC converters adopting switched-capacitor cell," *Industrial Electronics, IEEE Transactions on*, vol. PP, pp. 1–10, 2014.

[10] P. Xuewei and A. Rathore, "Novel bidirectional snubberless naturally commutated soft-switching current-fed

full-bridge isolated DC/DC converter for fuel cell vehicles," *Industrial Electronics, IEEE Transactions on*, vol. 61, no. 5, pp. 2307–2315, 2014.

[11] V. Valdivia, A. Barrado, A. Lazaro, M. Sanz, D. Lopez del Moral, and C. Raga, "Black-box behavioral modeling and identification of DC-DC converters with input current control for fuel cell power conditioning," *Industrial Electronics, IEEE Transactions on*, vol. 61, no. 4, pp. 1891–1903, 2014.

[12] K. C. Tseng and C. C. Huang, "High step-up high-efficiency interleaved converter with voltage multiplier module for renewable energy system," *Industrial Electronics, IEEE Transactions on*, vol. 61, no. 3, pp. 1311–1319, 2014.

[13] X. Hu and C. Gong, "A high gain input-parallel output-series DC/DC converter with dual coupled inductors," *Power Electronics, IEEE Transactions on*, vol. 30, no. 3, pp. 1306–1317, 2015.

[14] S. Burany, R. B. Gopal, N. A. Freeman, and S. Masse, "Method and apparatus for monitoring fuel cell voltages," American Patent US 7,148,654, 2006.

[15] M. Ordonez, M. Sonnaillon, J. Quaicoe, and M. Iqbal, "An embedded frequency response analyzer for fuel cell monitoring and characterization," *Industrial Electronics, IEEE Transactions on*, vol. 57, no. 6, pp. 1925–1934, 2010.

[16] F. A. de Bruijn, V. A. T. Dam, and G. J. M. Janssen, "Review: Durability and degradation issues of PEM fuel cell components," *Fuel Cells*, vol. 8, no. 1, pp. 3–22, 2008.

[17] W. Schmittinger and A. Vahidi, "A review of the main parameters influencing long-term performance and durability of PEM fuel cells," *Journal of Power Sources*, vol. 180, no. 1, pp. 1–14, 2008.

[18] B. Pregelj, D. Vrečko, and V. Jovan, "Improving the operation of a fuel-cell power unit with supervision control - a simulation study," *Journal of Power Sources*, vol. 196, no. 22, pp. 9419–9428, 2011.

[19] S. Silva, M. Severino, and M. de Oliveira, "A stand-alone hybrid photovoltaic, fuel cell and battery system: A case study of tocantins, brazil," *Renewable Energy*, vol. 57, pp. 384–389, 2013.

[20] A. J. Verhage, J. F. Coolegem, M. J. Mulder, M. H. Yildirim, and F. A. de Bruijn, "30,000 h operation of a 70 kW stationary PEM fuel cell system using hydrogen from a chlorine factory," *International Journal of Hydrogen Energy*, vol. 38, no. 11, pp. 4714–4724, 2013.

[21] B. Pregelj, D. Vrečko, J. Petrovčič, V. Jovan, and G. Dolanc, "A model-based approach to battery selection for truck onboard fuel cell-based APU in an anti-idling application," *Applied Energy*, vol. 137, pp. 64–76, 2015.

[22] X. Z. Yuan, H. Wang, J. C. Sun, and J. Zhang, "AC impedance technique in PEM fuel cell diagnosis – A review," *International Journal of Hydrogen Energy*, vol. 32, pp. 4365–4380, 2007.

[23] J. Wu, X. Z. Yuan, H. Wang, M. Blanco, J. J. Martin, and J. Zhang, "Diagnostic tools in PEM fuel cell research: Part I Electrochemical techniques," *International Journal of Hydrogen Energy*, vol. 33, no. 6, pp. 1735–1746, 2008.

[24] R. Petrone, Z. Zheng, D. Hissel, M. Péra, C. Pianese, M. Sorrentino, M. Becherif, and N. Yousfi-Steiner, "A review on model-based diagnosis methodologies for PEMFCs," *International Journal of Hydrogen Energy*, vol. 38, no. 17, pp. 7077–7091, 2013.

[25] Z. Zheng, R. Petrone, M. Péra, D. Hissel, M. Becherif, C. Pianese, N. Y. Steiner, and M. Sorrentino, "A review on non-model based diagnosis methodologies for PEM fuel cell stacks and systems," *International Journal of Hydrogen Energy*, vol. 38, no. 21, pp. 8914–8926, 2013.

[26] S. M. Rezaei Niya and M. Hoorfar, "Study of proton exchange membrane fuel cells using electrochemical impedance spectroscopy technique – A review," *Journal of Power Sources*, vol. 240, pp. 281–293, 2013.

[27] X. Z. Yuan, C. Sons, H. Wang, and J. Zhang, *Electrochemical Impedance Spectroscopy in PEM Fuel Cells, Fundamentals and Applications*. London: Springer, 2010.

[28] A. Debenjak, P. Boškoski, B. Musizza, J. Petrovčič, and Đ. Juričić, "Fast measurement of proton exchange membrane fuel cell impedance based on pseudo-random binary sequence perturbation signals and continuous wavelet transform," *Journal of Power Sources*, vol. 254, pp. 112–118, 2014.

[29] P. Boškoski and A. Debenjak, "Optimal selection of proton exchange membrane fuel cell condition monitoring thresholds," *Journal of Power Sources*, vol. 268, pp. 692–699, 2014.

[30] G. Terzulli and B. W. Peace, *Film technology to replace electrolytic technology*, AVX, 2004.

[31] H. Wang and F. Blaabjerg, "Reliability of capacitors for DC-link applications in power electronic converters–an overview," *Industry Applications, IEEE Transactions on*, vol. 50, no. 5, pp. 3569–3578, Sept 2014.

[32] T. L. Skvarenina, Ed., *The Power Electronics Handbook*, ser. Industrial Electronics. CRC Press, 2001.

[33] W. A. Kester, *Analog Devices Practical Design Techniques For Power And Thermal Management, Analog Devices technical reference books*. Analog Devices, 1998.

[34] *Modulated Constant off-Time Control Mechanism, Application Note*. Linfinity Microelectronics, 1998.

[35] S. H. Chee, *A New, High Efficiency Monolithic Buck Converter*. Linear Technology, 1995.

[36] D. Webb and S. Moeller-Holst, "Measuring individual cell voltages in fuel cell stacks," *Journal of Power Sources*, vol. 103, pp. 54–60, 2001.

[37] D. Brunner, A. K. Prasad, S. G. Advani, and B. W. Peticolas, "A robust cell voltage monitoring system for analysis and diagnosis of fuel cell or battery systems," *Journal of Power Sources*, vol. 195, no. 24, pp. 8006–8012, 2010.

[38] B. Dobkin and J. Williams, Eds., *Analog Circuit Design - A Tutorial Guide to Applications and Solutions*. Elsevier, 2011.

[39] S. Mallat, *A Wavelet Tour of Signal Processing: The Sparse Way*, 3rd ed. Burlington, MA: Elsevier Academic

Press, 2008.

[40] I. Daubechies, *Ten Lectures on Wavelets*, ser. CBMS-NSF Regional Conference Series in Applied Mathematics. Society for Industrial and Applied Mathematics, 1992.

[41] E. O. Doebelin, *System Modeling and Response*. John Wiley & Sons Inc, 1980.

[42] P. O. Amblard, M. Gaeta, and J. L. Lacoume, "Statistics for complex variables and signals - part i: Variables," *Signal Processing*, vol. 53, pp. 1–13, 1996.

[43] N. Goodman, "Statistical analysis based on a certain multivariate complex gaussian distribution," *The Annals of mathematical statistics*, vol. 34, no. 1, pp. 152–177, 1963.

[44] E. Ollila, "On the circularity of a complex random variable," *IEEE Signal Processing Letters*, vol. 15, pp. 841–844, 2008.

[45] A. Khurshid, Z. Al-Hemyari, and S. Kamal, "On complex random variables," *Pakistan Journal of Statistics and Operation Research*, vol. 8, no. 3, pp. 645–654, 2012.

[46] R. J. Baxley, B. T. Walkenhorst, and G. Acosta-Marum, "Complex gaussian ratio distribution with applications for error rate calculation in fading channels with imperfect CSI," in *IEEE GLOBECOM 2010*, 2010.

[47] M. K. Simon, *Probability Distributions Involving Gaussian Random Variables*. New York: Springer Science, 2006.

[48] E. Bechhoefer and A. Bernhard, "A generalized process for optimal threshold setting in HUMS," in *IEEE Aerospace Conference*, 2007.

[49] N. Fouquet, C. Doulet, C. Nouillant, G. Dauphin-Tanguy, and B. Ould-Bouamama, "Model based PEM fuel cell state-of-health monitoring via AC impedance measurements," *Journal of Power Sources*, vol. 159, pp. 905–913, 2006.

[50] J. M. Le Canut, R. M. Abouatallah, and D. A. Harrington, "Detection of membrane drying, fuel cell flooding, and anode catalyst poisoning on PEMFC stack by electrochemical impedance spectroscopy," *Journal of The Electrochemical Society*, vol. 153, pp. A857–A864, 2006.

[51] M. Rubio, A. Urquia, and S. Dormido, "Diagnosis of performance degradation phenomena in PEM fuel cells," *International Journal of Hydrogen Energy*, vol. 35, no. 7, pp. 2586–2590, 2010.

[52] A. Debenjak, M. Gašperin, B. Pregelj, M. Atanasijević-Kunc, J. Petrovčič, and V. Jovan, "Detection of flooding and drying inside a PEM fuel cell stack," *Strojniški vestnik - Journal of Mechanical Engineering*, vol. 59, no. 1, pp. 56–64, 2013.

[53] J. Kim, I. Lee, Y. Tak, and B. Cho, "Impedance-based diagnosis of polymer electrolyte membrane fuel cell failures associated with a low frequency ripple current," *Renewable Energy*, vol. 51, pp. 302–309, 2013.

[54] S. Tant, S. Rosini, P. X. Thivel, F. Druart, A. Rakotondrainibe, T. Geneston, and Y. Bultel, "An algorithm for diagnosis of proton exchange membrane fuel cells by electrochemical impedance spectroscopy," *Electrochimica Acta*, vol. 135, pp. 368–379, 2014.

[55] M. Gašperin, P. Boškoski, A. Debenjak, and J. Petrovčič, "Signal processing and stochastic filtering for EIS based PHM of fuel cell systems," *Fuel Cells*, vol. 14, no. 3, pp. 457–465, 2014.

[56] G. Dotelli, R. Ferrero, P. Stampino, S. Latorrata, and S. Toscani, "Diagnosis of PEM fuel cell drying and flooding based on power converter ripple," *Instrumentation and Measurement, IEEE Transactions on*, vol. 63, no. 10, pp. 2341–2348, 2014.

[57] R. Isermann and M. Münchhof, *Identification of Dynamic Systems: An Introduction with Applications*, ser. Advanced textbooks in control and signal processing. Springer-Verlag Berlin Heidelberg, 2011.